IGARSS 2023 - 2023 IEEE International Geoscience and Remote Sensing Symposium | 979-8-3503-2010-7/23/$31.00 ©2023 IEEE | DOI: 10.1109/IGARSS52108.2023.10281795

B1D–CNN: A NOVEL CONVOLUTION NEURAL NETWORK-BASED CHLOROPHYLL-A RETRIEVAL ALGORITHM FOR SENTINEL–2 DATA

Muhammad Salah, Hiroto Higa, Joji Ishizaka, Salem Ibrahim Salem
Graduate School of Engineering, Kyoto University of Advanced Science

ABSTRACT

Deep learning (DL) methods have been recently considered suitable for Chlorophyll-a (Chla) retrieval from satellite data due to their ability for handling complex, high-dimensional, and noisy data. This manuscript describes B1D–CNN, a new model combining 1D-convolutional neural networks (1D-CNN) and a traditional empirical blend algorithm to estimate Chla using the MultiSpectral Instrument (MSI) sensor on board the Sentinel-2 satellite. The proposed model is trained and evaluated against the state-of-the-art Mixture Density Network (MDN) and the classical Chla retrieval algorithms using global in-situ data. The results show a 9.25% to 54.12% improvement in the RMSE, along with a 3.45% to 59.53% reduction in the MAE. A satellite image during a harmful algal bloom (HABs) event was also assessed using B1D–CNN, and the proposed model captured the high Chla batches associated with HABs. This study indicates the advantages of using DL methods to retrieve Chla.

Index Terms— Chlorophyll-a, CNN, MSI, Ocean Color

1. INTRODUCTION

Chlorophyll-a (Chla) is a pigment found in phytoplankton, the microscopic plants that form the base of the oceanic food web [1]. Changes in Chla concentrations can indicate changes in the productivity and biodiversity of an ecosystem, as well as potential impacts from anthropogenic activities such as pollution and climate change [2], [3]. The need for a global Chla retrieval algorithm from satellite remote sensing data is critical for monitoring and understanding the health of aquatic ecosystems.

Researchers have been developing empirical and semi-analytical algorithms that relate remote sensing reflectance (Rrs) bands to the Chla concentrations [4], [5]. However, the relationship between Rrs bands and Chla concentrations is complex, particularly in turbid waters. The Rrs signal is affected not only by phytoplankton but also other water constituents such as colored dissolved organic matter [6]. Most of Chla algorithms rely on a combination of statistical methods and empirical techniques, for instance, band ratio algorithms are typical examples that apply linear, polynomial or power functions to retrieve Chla. These algorithms rely on the ratio between blue and green bands for case-1 waters [7], [8] or near-infrared (NIR) bands and red bands to infer Chla concentrations in case-2 waters [9], [10]. Band ratio algorithms can be divided into different categories based on the number of bands used, including 2-Bands [11], 3-Bands [12], and 4-Bands [13] algorithms.

Ocean Color (OCx) algorithms developed by NASA's Ocean Biology Processing Group (OBPG) are widely used for Chla retrieval from satellite data [8], [14], [15]. The OCx algorithms are fourth-order polynomial equations that model the non-linear relationship between Rrs and Chla. For example, the OC3 algorithm uses the ratio between three bands in the blue-green wavelengths to estimate Chla concentrations [8]. The current NASA standard Chla product is a merge of the OCx algorithm, and the color index (CI) algorithm known as the OCI algorithm [16], designed for case 1 waters. Other combinations of algorithms, such as the blend algorithm, which merges the 2-Bands algorithm with OC3, have also been developed for both case-1 and case-2 waters [17].

Machine learning (ML) and deep learning (DL) methods have been increasingly considered in recent years for modeling and retrieving Chla concentrations from satellite data [18]. These methods have the advantage of handling large and complex datasets and learning non-linear relationships between Rrs and Chla concentrations.

ML methods, such as Random Forest [19]–[21], Support Vector Machine (SVM) [19], [20], [22], [23], and k-Nearest Neighbors (k-NN) [19], [20], have been tested for Chla retrieval and showed possible results. DL methods, such as Feed-forward Networks [24], [25], Convolutional Neural Networks (CNNs) [26], and Mixture Density Networks (MDN) [27]–[29] have also been used for Chla retrieval. These models use multiple layers of artificial neurons with different architectures to model complex non-linear relations.

To the best of the authors' knowledge, previous ML models for Chla retrieval have not considered the classification of Chla into different eutrophic states, resulting in less precise generalized algorithms. Therefore, this research presents a new Chla retrieval model that combines the empirical blend algorithm (OC3 and 2-Bands) with a 1D–CNN network. The 1D–CNN is particularly effective for modeling sequential data such as Rrs. The Blend algorithm provides an initial estimate of Chla, which is used for classifying the Chla into three classes, whereas the 1D–CNN model generates more accurate estimates within each class. Thus, the aim of this study is (a) to evaluate the B1D–CNN model in comparison with other well-established Chla algorithms using a comprehensive global dataset and (b) to assess the model's ability to capture the harmful algal blooms (HABs) distribution via satellite imagery during HABs outbreaks.

2. DATA

The study incorporates the GLORIA dataset [30], [31], a global in-situ measurements of hyperspectral Rrs, and the corresponding Chla concentrations. Additionally, a dataset with measurements from multiple water bodies in Japan, Vietnam, and Thailand is also used. A total of 4,739 hyperspectral Rrs-Chla pairs were considered. The Chla distribution shown in Figure 1 emphasizes the diversity in the Chla concentrations, which range from 0.031 to 148.84 mg/m^3, with a mean of 18.97 and a standard deviation (std) of 22.94. The Sentinel-2 MSI [32] Level-1C radiance-calibrated products were obtained from the Copernicus Open Access Hub (https://scihub.copernicus.eu). Level-1C products were then resampled to a 10 m resolution and atmospherically corrected using the Case-2 Regional CoastColour (C2RCC) processor [33]. The processing of all images was conducted using NASA SeaDAS software version 8.3. To evaluate the B1D–CNN model on satellite data, a Level-1C MSI image captured on Sep. 16, 2021, during a harmful algal bloom event near the northeast coast of Hokkaido, Japan, was downloaded and processed (Figure 4a).

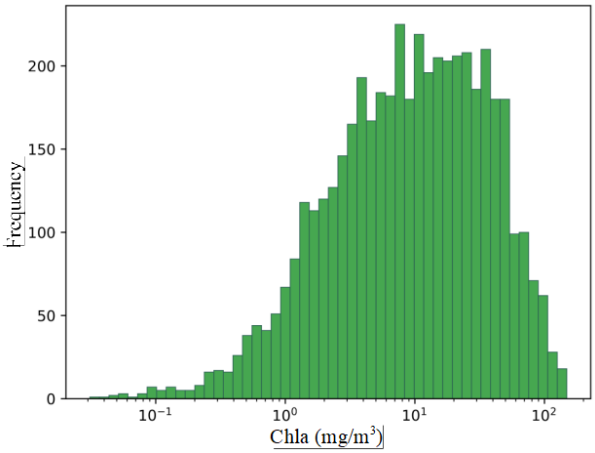

Figure 1. Chlorophyll-a distribution histogram for the 4739 data samples with a mean of 18.97 and std of 22.94.

3. MODEL DEVELOPMENT

The proposed model for Chla retrieval is a multi-stage architecture that combines traditional and DL methods to handle the problem's complexity and provide more accurate results. The model shown in Figure 2 comprises two main parts: an empirical model and three DL estimators based on the 1D CNNs. The empirical algorithm, namely the blend algorithm [17], provides an initial estimate of the Chla class (low, moderate, or high) based on the input Rrs values. Once the Chla class is determined, the Rrs values are then fed into one of the three estimators, each of which is specifically trained for the corresponding Chla class. These networks are used to obtain a fine-tuned Chla estimate and improve the Chla retrieval's accuracy.

3.1. Feature Engineering

Before training the estimators and using them, the data goes through several steps of feature engineering and normalization on the fly: (i) the significant bands of the MSI sensor (namely the visible and NIR bands: 443, 490, 560, 665, 705, 740, 783) are fetched from the input data, and missing data are filtered out, (ii) the Isolation Forest anomaly detection algorithm [34] is applied to ensure a unified distribution of the data, and (iii) normalization is done by applying log transformation for the input reflectance.

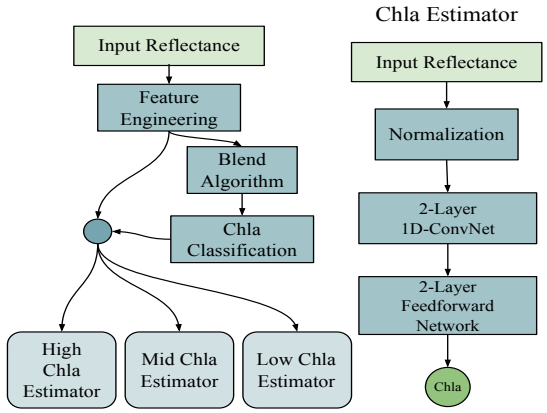

Figure 2. Overall system architecture with three DL estimators and empirical classifier

3.2. Deep Learning Estimators

The architecture of each DL estimator shown in Figure 2 comprises three main parts: normalization, encoding, and decoding. The encoding step is where the normalized Rrs data is fed into a 2-layered 1D-CNN that captures the relationship between the input reflectance and the output Chla considering the sequential nature of the reflectance values, encoding the input values to an intermediate vector representation of Rrs. In the decoding step, the vector obtained from the encoding step is fed into a 2-layered fully connected feed-forward

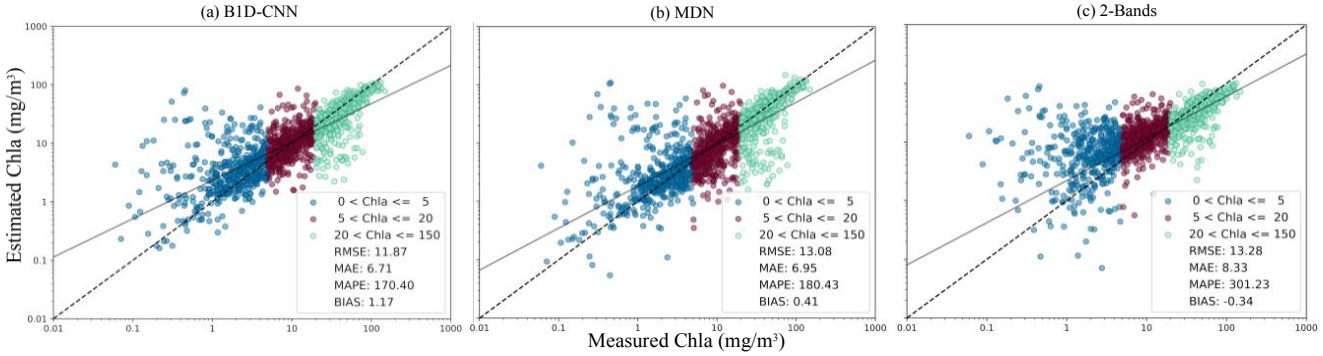

Figure 3: Scatterplots of the top 3 Chla retrieval models: (a) B1D–CNN, (b) MDN, and (c) 2-Band algorithm, highlighting Chla ranges of low (0-5 mg/m³), moderate (5-20 mg/m³), and high (20-150 mg/m³) in blue, brown, and green, respectively.

network with an output layer. This step attempts to estimate the Chla concentration value accurately.

3.3. Evaluating Chla Algorithms

Among the well-known standard algorithms for Chla retrieval from the MSI reflectance data, six algorithms were selected: the 3 bands version of the Ocean Color algorithm (OC3) [8], the OCI algorithm [16], which uses a combination of the Color Index algorithm (CI) and the OC3 algorithm, 2-Bands [10], [11], 3-band [12], 4-band [13], and the Blend algorithm [17]. The Blend algorithm combines the 2-Bands ratio algorithm with the OC3 algorithm. In addition to the classic algorithms, B1D–CNN is also compared to the state-of-art DL model based on the Mixture Density Network (MDN) architecture [27].

The metrics used for the evaluation of B1D–CNN and the above-mentioned algorithms are mainly: root mean squared error (RMSE), mean absolute error (MAE), mean absolute percentage error (MAPE), and the Bias.

4. RESULTS AND DISCUSSION

4.1. Performance Evaluation on In-Situ Data

The overall performance (Table 1) indicates that the B1D–CNN model outperforms other evaluated Chla models, showcasing the lowest RMSE, MAE and MAPE values. It substantially enhanced prediction accuracy compared to the poorest-performing models, OC3 and OCI, reducing RMSE by approximately 54%, MAE by about 52% and the MAPE by 4-folds. The top-performing models are B1D–CNN, MDN, and the 2-Bands algorithm, with RMSE of 11.87, 13.08, and 13.28 mg/m^3, respectively. Conversely, the 3-Bands and 4-Bands models exhibited the highest MAPE values, indicating inadequate performance.

model	RMSE	MAE	MAPE	BIAS
B1D–CNN	**11.87**	**6.71**	**170.40**	1.17
MDN	13.08	6.95	180.43	**0.41**
OC3	25.87	13.95	287.71	-0.77
OCI	25.87	13.95	287.68	-0.77
2-Bands	13.28	8.33	301.23	-0.34
3-Bands	22.03	16.63	669.44	-1.79
4-Bands	21.98	16.58	676.56	-1.75
Blend	14.46	9.13	274.77	-0.60

Table 1. Overall performance evaluation of all Chla models.

The scatter plots of Figure 3 visually illustrate the detailed evaluation of the top-performing models. The plots are divided into three Chla ranges: low (0-5 mg/m^3), moderate (5-20 mg/m^3), and high (20-150 mg/m^3). Some data points show the same error among the three plots, which could be attributed to uncertainty in those samples. In general, as shown in Table 2, the DL models have similar results in the high Chla range, but compared to the 2-Bands the MDN and B1D–CNN have significantly higher performance, this indicates that DL models have better abilities to model high Chla ranges than classical algorithms.

In the mid and low Chla ranges, B1D–CNN significantly reduces the error compared to the two other models, achieving a 5.4% to 15.2% lower RMSE and a 11.6% to 19.5% reduction in the MAE in the moderate range. On the other hand, the 2-Bands algorithm gives lower RMSE than MDN in the mid-range. For the low Chla range, DL models, again, outperform the 2-Bands algorithm with almost 2 folds with respect to the MAE. Furthermore, B1D–CNN has a significantly lower RMSE of 8.33 compared to 10.83 and 11.45 of MDN and 2-Bands, respectively. These results could be attributed to the inherent nature of 2-Bands algorithms, which is specifically designed for moderate turbid waters [10], [35].

Chla	model	RMSE	MAE	MAPE	BIAS
0-5 (mg/m^3)	B1D–CNN	**8.33**	**3.56**	**435.56**	**-3.10**
	MDN	10.83	3.69	459.55	-3.10
	2-Bands	11.45	6.69	813.96	-5.72
5-20 (mg/m^3)	B1D–CNN	**8.28**	**4.51**	**46.45**	-1.40
	MDN	9.76	5.10	51.52	**-0.96**
	2-Bands	8.75	5.60	62.32	-4.16
20-150 (mg/m^3)	B1D–CNN	**17.38**	12.67	30.12	8.74
	MDN	17.80	**12.62**	30.95	**5.77**
	2-Bands	18.46	13.29	**29.10**	9.89

Table 2. Performance evaluation of top 3 Chla retrieval models at different Chla ranges.

4.2. Applying to Satellite Data

The top-performing models were evaluated using a satellite image captured during a harmful algal bloom (HAB) event (Figure 4a). The image was taken during the HAB event to assess the models' ability to identify and detect these events from satellite imagery. The results of this evaluation are demonstrated in Figure 4, which shows that the DL models can accurately detect HAB patches in the image and provide high Chla concentrations corresponding to those patches. On the other hand, the 2 bands algorithm failed to obtain the Chla concentration in some patches and showed lower abilities in

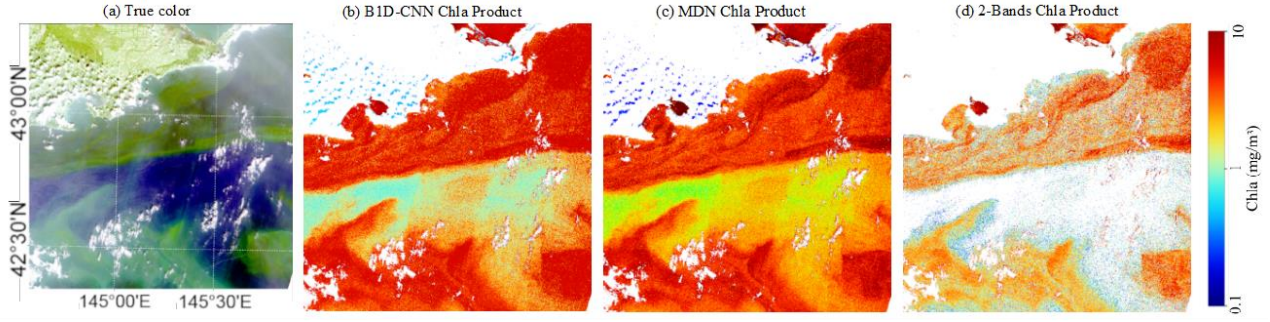

Figure 4. (a) True color image of Harmful algal blooms batches near the northeast coast of Hokkaido, Japan. Chla retrieved using the top 3 models (b) B1D–CNN, (c) MDN, and (d) 2-Bands algorithm.

capturing high Chla patches. This highlights the model's ability to effectively identify and detect HABs using satellite imagery, which can be helpful in monitoring and studying aquatic ecosystems.

5. CONCLUSION

This study presents B1D–CNN, a novel deep learning model combining 1D-convolutional neural networks and the empirical blend algorithm, for estimating Chlorophyll-a (Chla) from Sentinel-2 satellite data. B1D–CNN was evaluated using a global dataset against state-of-the-art models. The proposed model demonstrated significant improvements in accuracy, with a 9.25% to 54.12% improvement in the RMSE. Additionally, the B1D–CNN successfully detected high Chla batches in satellite imagery during a harmful algal bloom event, highlighting its potential as an effective tool for monitoring aquatic ecosystems. This research highlights the benefits of using deep learning models for Chla retrieval from satellite data.

11. REFERENCES

[1] P. G. Falkowski, E. A. Laws, R. T. Barber, and J. W. Murray, in *Ocean Biogeochemistry*, Berlin, Heidelberg: Springer Berlin Heidelberg, 2003, pp. 99–121. doi: 10.1007/978-3-642-55844-3_5.

[2] V. H. Smith, *J Plankton Res*, vol. 29, no. 1, pp. 1–6, Oct. 2006, doi: 10.1093/plankt/fbl061.

[3] J. Carstensen, M. Sánchez-Camacho, C. M. Duarte, D. Krause-Jensen, and N. Marbà, *Environ Sci Technol*, vol. 45, no. 21, pp. 9122–9132, Nov. 2011, doi: 10.1021/es202351y.

[4] D. Odermatt, A. Gitelson, V. E. Brando, and M. Schaepman, *Remote Sens Environ*, vol. 118, pp. 116–126, Mar. 2012, doi: 10.1016/J.RSE.2011.11.013.

[5] S. Salem *et al.*, *Remote Sens (Basel)*, vol. 9, no. 6, p. 556, Jun. 2017, doi: 10.3390/rs9060556.

[6] K. D. Menken, P. L. Brezonik, and M. E. Bauer, *Lake Reserv Manag*, vol. 22, no. 3, pp. 179–190, Sep. 2006, doi: 10.1080/07438140609353895.

[7] S. Hooker *et al.*, May 2000.

[8] J. E. O'Reilly and P. J. Werdell, *Remote Sens Environ*, vol. 229, pp. 32–47, Aug. 2019, doi: 10.1016/j.rse.2019.04.021.

[9] K.-H. Mittenzwey, S. Ullrich, A. A. Gitelson, and K. Y. Kondratiev, *Limnol Oceanogr*, vol. 37, no. 1, pp. 147–149, Jan. 1992, doi: 10.4319/lo.1992.37.1.0147.

[10] H. J. Gons, *Environ Sci Technol*, vol. 33, no. 7, pp. 1127–1132, Apr. 1999, doi: 10.1021/es9809657.

[11] A. A. Gilerson *et al.*, *Opt Express*, vol. 18, no. 23, p. 24109, Nov. 2010, doi: 10.1364/OE.18.024109.

[12] G. Dall'Olmo, A. A. Gitelson, and D. C. Rundquist, *Geophys Res Lett*, vol. 30, no. 18, Sep. 2003, doi: 10.1029/2003GL018065.

[13] C. Le, Y. Li, Y. Zha, D. Sun, C. Huang, and H. Lu, *Remote Sens Environ*, vol. 113, no. 6, pp. 1175–1182, Jun. 2009, doi: 10.1016/j.rse.2009.02.005.

[14] J. E. O'Reilly *et al.*, *J Geophys Res Oceans*, vol. 103, no. C11, pp. 24937–24953, Oct. 1998, doi: 10.1029/98JC02160.

[15] J. E. O'Reilly *et al.*, *SeaWiFS postlaunch calibration and validation analyses, Part*, vol. 3, pp. 9–23, 2000.

[16] C. Hu, Z. Lee, and B. Franz, *J Geophys Res Oceans*, vol. 117, no. C1, Jan. 2012, doi: 10.1029/2011JC007395.

[17] M. E. Smith, L. Robertson Lain, and S. Bernard, *Remote Sens Environ*, vol. 215, pp. 217–227, Sep. 2018, doi: 10.1016/j.rse.2018.06.002.

[18] S. Hafeez *et al.*, *Remote Sens (Basel)*, vol. 11, no. 6, p. 617, Mar. 2019, doi: 10.3390/rs11060617.

[19] L. Silveira Kupssinskü *et al.*, *Sensors*, vol. 20, no. 7, p. 2125, Apr. 2020, doi: 10.3390/s20072125.

[20] P. M. Maier and S. Keller, *ISPRS Annals of the Photogrammetry, Remote Sensing and Spatial Information Sciences*, vol. IV-2/W5, pp. 609–614, May 2019, doi: 10.5194/isprs-annals-IV-2-W5-609-2019.

[21] D. DIOUF and D. Seck, *International Journal of Artificial Intelligence & Applications*, vol. 10, no. 6, pp. 33–40, Nov. 2019, doi: 10.5121/ijaia.2019.10603.

[22] Haigang Zhan, Ping Shi, and Chuqun Chen, *IEEE Transactions on Geoscience and Remote Sensing*, vol. 41, no. 12, pp. 2947–2951, Dec. 2003, doi: 10.1109/TGRS.2003.819870.

[23] R. Matarrese, A. Morea, K. Tijani, V. de Pasquale, M. T. Chiaradia, and G. Pasquariello, in *IGARSS 2008 - 2008 IEEE International Geoscience and Remote Sensing Symposium*, 2008, pp. IV-910-IV–913. doi: 10.1109/IGARSS.2008.4779871.

[24] S. Graban, G. Dall'Olmo, S. Goult, and R. Sauzède, *Opt Express*, vol. 28, no. 16, p. 24214, Aug. 2020, doi: 10.1364/OE.397863.

[25] D. Gómez, P. Salvador, J. Sanz, and J. L. Casanova, *Environmental Pollution*, vol. 286, p. 117489, Oct. 2021, doi: 10.1016/j.envpol.2021.117489.

[26] D. Jin, E. Lee, K. Kwon, and T. Kim, *Remote Sens (Basel)*, vol. 13, no. 10, p. 2003, May 2021, doi: 10.3390/rs13102003.

[27] N. Pahlevan *et al.*, *Remote Sens Environ*, vol. 240, p. 111604, Apr. 2020, doi: 10.1016/j.rse.2019.111604.

[28] N. Pahlevan *et al.*, *Remote Sens Environ*, vol. 270, p. 112860, Mar. 2022, doi: 10.1016/j.rse.2021.112860.

[29] B. Smith *et al.*, *Frontiers in Remote Sensing*, vol. 1, Feb. 2021, doi: 10.3389/frsen.2020.623678.

[30] R. Spang, J. J. Remedios, and M. P. Barkley, *Advances in Space Research*, vol. 33, no. 7, pp. 1041–1047, Jan. 2004, doi: 10.1016/S0273-1177(03)00585-4.

[31] S. Johansson *et al.*, *Atmos Meas Tech*, vol. 11, no. 8, pp. 4737–4756, Aug. 2018, doi: 10.5194/amt-11-4737-2018.

[32] M. Drusch *et al.*, *Remote Sens Environ*, vol. 120, pp. 25–36, May 2012, doi: 10.1016/j.rse.2011.11.026.

[33] C. Brockmann, R. Doerffer, M. Peters, S. Kerstin, S. Embacher, and A. Ruescas, in *Living Planet Symposium*, Aug. 2016, vol. 740, p. 54.

[34] F. T. Liu, K. M. Ting, and Z.-H. Zhou, in *2008 Eighth IEEE International Conference on Data Mining*, Dec. 2008, pp. 413–422. doi: 10.1109/ICDM.2008.17.

[35] S. Salem, H. Higa, H. Kim, H. Kobayashi, K. Oki, and T. Oki, *Sensors*, vol. 17, no. 8, p. 1746, Jul. 2017, doi: 10.3390/s17081746.